Available online at www.CivileJournal.org

Civil Engineering Journal

(E-ISSN: 2476-3055; ISSN: 2676-6957)

Vol. 9, No. 10, October, 2023

Modeling of Heat Transfer in Massive Concrete Foundations Using 3D-FDM

Dina M. Mansour [1*], Ahmed M. Ebid [1]

[1] *Structural Eng. and Constr. Management Department, Faculty of Engineering and Technology, Future University in Egypt, Cairo, Egypt.*

Received 15 January 2023; Revised 24 August 2023; Accepted 09 September 2023; Published 01 October 2023

Abstract

Analyzing and modeling the thermal behavior of mass concrete elements has been widely investigated by several researchers. Lately, many contemporary finite element packages have embedded modules for analyzing thermal behavior. Unfortunately, these packages are quite complex and require experts to be properly implemented. This paper proposes a simple and practical approach using the 3D-Finite Difference Model (3D-FDM) developed by MS-Excel to overcome the complexity of the other FE models. The model is utilized to predict the thermal behavior of actual bridge pile caps (3D model) rather than the previously developed 2D models in earlier research. The results of the analysis are compared with the concrete temperatures that were experimentally obtained from the site. Site data was collected using 18 thermocouple probes (K type) that were installed in two pile caps. These thermocouples were installed before concrete pouring to monitor the temperatures generated due to the exothermic reaction of the cement, which occurs during casting and the maturity period of concrete. The readings were registered every 3 hours for 7 days after concrete placement. This research provides a comparison between the recorded site data and the thermal analysis based on the proposed 3D-FDM. Results proved that concrete temperature time histories at different locations of the bridge pile caps could be properly predicted using the developed 3D-FDM.

Keywords: 3D-Finite Difference; Mass Concrete; Thermal Analysis; Bridge Pile Caps; Thermal Modeling.

1. Introduction

Concrete is globally used as a practical and economical material in different construction projects, especially for infrastructure projects such as bridges. Hence, mass concrete abutments, piers, and pile caps are constructed to satisfy bridges' crossing capacities [1, 2]. Mass concrete is defined as any concrete element with dimensions large enough to require extra precautions to avoid excessive heat caused by cement hydration and cracking [3]. Cement particles emit large amounts of heat, known as heat of hydration, after coming into contact with water [4]. The temperature is high in the middle section of mass concrete elements at early ages and lower in the outer parts [5].

Concrete's core temperature rises rapidly in the first few days. On the other hand, the element's surface dissipates heat into the adjacent environment, which causes a steep temperature variation between the core and the exposed surfaces. This irregular temperature distribution causes volumetric changes during the early age of concrete, which creates tensile strains and stresses within the concrete mass [6]. The heat inside the concrete block results in tensile stresses in situations where concrete cannot move freely. If these tensile stresses exceed the concrete's tensile strength, tightness, cracking, and possible damage to the concrete element can occur, which will eventually affect the service life of the structure [7, 8].

* Corresponding author: dmohamed@fue.edu.eg

http://dx.doi.org/10.28991/CEJ-2023-09-10-05

Temperature cracks appear in mass concrete elements as a result of temperature stresses exceeding the critical ones. These cracks affect and destroy the stability and integrity of the structure [9]. Previous research stated that analyzing the heat of hydration of mass concrete structures is hard due to the fact that they have several heat transfer properties and several materials [10]. Hence, the temperature change is a significant parameter that should be considered in the research, design, and construction of mass structures, as illustrated by Zhang et al. [11].

The Portland Cement Association [12] assured that the rate of heat generation is greatest at early ages. The greatest rate of heat liberation takes place within the first 24 hours, and a large amount of heat is produced within the first 3 days. Therefore, a thermal control plan is mandated for mass concrete elements by installing thermal sensors and monitoring the temperatures in certain locations within the concrete mass. If internal temperatures surpass 70°C, micro-cracking will occur, causing durability issues due to internal deterioration [13–15].

To cope with the prompt schedules of the construction industry, contractors have recently started to use high-binder content concrete mixtures, allowing for early-age strength to speed up formwork removal. As a result of increasing the amount of cement in the concrete mix, both the temperature gradient between the surface and the core and the peak temperature increase. This indicates comparable behavior to mass concrete [16]. During the first few days after casting concrete, the potential temperature difference causes high-temperature gradients, particularly in cases of significant temperature variations between day and night. The interior of the concrete can reach as high as 70° C, while the surface cools down very fast due to ambient temperature. Gajda [17], Leon & Chen [18] also stated that the thermal behavior of concrete elements is affected by the thermal properties of aggregates, size of the structure, type of formwork, location, insulation, and ambient conditions as well. Other researchers noticed that concrete's thermal properties are not affected by age and that the type of coarse aggregate has a great effect on conductivity, while the original water content has less effect [19]. In mass concrete elements, concrete thermal modeling gives designers and contractors the opportunity to estimate the elevation of temperature within concrete elements before pouring, which allows them to adapt their construction and production techniques to handle and manage these circumstances [20].

Several researchers [13, 20, 21] mentioned different techniques that can be used to minimize the thermal gradients and peak temperatures as well, like cooling the concrete components to reduce the concrete's initial temperature, selecting convenient aggregates with a low coefficient of thermal expansion, using modified or low-heat cement, using nitrogen cooling, pipe cooling, insulated formwork, or using thermal blankets to insulate the concrete element. These are the most effective and economical precautions that can be implemented to control early-age cracking [22, 23]. Since it is intractable to run such precautions during construction, it is possible to predict the development of temperature in advance so that appropriate precautions can be preplanned and implemented accordingly. Consequently, temperature-time prediction histories of mass concrete structures have become of significant concern for both project engineers and contractors, as mentioned by Maruyama & Lura [24] and Chu et al. [25].

2. Finite Element and Finite Difference Modeling in Previous Research

Many techniques and tools were used to predict the temperature-time history of mass concrete structures. Schmidt’s technique and Carlson’s technique were utilized before the computer era, applying simplified finite difference solutions to specify the single nodes' temperatures in time increments. In both techniques, concrete was split into small elements, and each element's temperature was deemed to be the average of the surrounding elements' temperatures [26].

In the 1930s, the Schmidt technique was presented as a simple FDM to calculate the temperature rise in concrete structures. The Schmidt technique was also the foundation for many finite element packages [27]. Recently, spreadsheet programs have been used to perform such repeated calculations more accurately [28]. Additionally, the Finite Difference Method (FDM) can predict temperature histories in large concrete elements using a built-in macro developed using a spreadsheet. To overcome the differences in heat generated, another spreadsheet program applying Schmidt’s method using an empirical prediction model was proposed [7, 29].

In 2004, research proposed a 2D finite difference solution to the heat equations to model the profiles of the time-based temperatures. But it had the strong limitation of developing only a 2D model, yet it was an improvement to the Schmidt technique as it considered the hydrating cement heat escalation [30]. Also, the authors stated that wide research was conducted using FEM, and a couple of studies extended the 2D modeling technique of thermal behavior into a 3D model.

FEM has proven to be an outstanding theoretical base in engineering and scientific applications by providing reliability and accuracy, as mentioned by Zhu et al. [31]. Different models and programs were developed to predict the temperature elevation in concrete. Some were designed for mass elements, while others could be used for any element. But it has to be kept in mind that computer models for predicting heat rise can be a little cost-effective for some countries [27]. The authors also discussed several sophisticated tools, but it was noted that the users must have a

strong background in hydration and cement chemistry to be able to utilize these tools properly with convenient assumptions. Moreover, uploading other materials and new cement types will necessitate a highly detailed analysis.

Contemporary researchers presented computer programs that predicted concrete temperatures by applying the Finite Difference and Finite Element Models to analyze the resulting thermal stresses [32, 33]. Some of these programs took into consideration different aspects such as the properties of constituent materials, concrete mixture ratios, building geometry, formwork type, curing alternatives, and environmental circumstances for temperature and crack predictions [34–36]. Commercial finite element-based software packages were also used to analyze mass concrete elements' thermal behavior. FEM-based software was applied to imitate the cold-water pipe-cooling technique, which decreased the temperature elevation in a massive bridge element. The influence of formwork type was investigated as well, using a FEM-based model to emulate the mass concrete elements' external heat loss and incorporating a convection model for the surface of the formwork made of steel. Additionally, to achieve more reliable outcomes, initial values and boundary conditions should be determined to consider field conditions. Factors like ambient conditions, initial concrete temperature, type of formwork used, and the time of formwork removal should be considered, as mentioned by Yikici & Chen [37].

Ultimately, it can be concluded that a great number of temperature prediction studies have been developed, but a practical and simple tool that can be used in developing countries is still missing. Consequently, the lack of decision-making in the construction industry in these countries regarding formwork removal time, insulation practices, precooling, and post-cooling techniques is up-to-the-minute. To close this gap, this research introduces an alternative approach for institutions in developing countries that can reasonably predict the thermal behavior of mass concrete elements.

3. Objectives

Although many earlier researchers investigated the thermal behavior of massive concrete elements using numerical models, these models are complicated and necessitate experts to be used properly. This research presents a simple and practical approach to creating a 3D-Finite Difference Model using MS-Excel. The proposed model can predict the thermal behavior of actual bridge pile caps (3D model). Moreover, a comparison between the recorded site data using 18 thermocouples and the thermal analysis based on the proposed 3D-FDM is introduced. Figure 1 demonstrates the methodology of this research in order to fulfill the previously mentioned objectives.

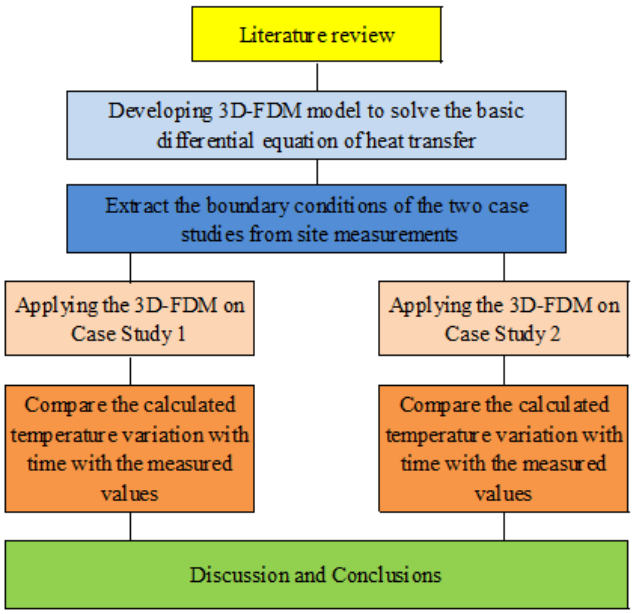

Figure 1. Flowchart of the research methodology

4. Project Overview

4.1. High Speed Railway Project

High-asset-value projects are widely constructed lately in developing countries as they introduce dynamic additions to the countries' road and highway networks [38, 39]. The "High-Speed Railway" (HSR) project is a modern railway network that connects Al Ain Sokhna City on the Red Sea coast with New Alamein City on the Mediterranean Sea coast, passing through the New Capital and Alexandria, as shown in Figure 2. The railway mainly rests on earth embankments, except for some local zones and intersections where it is supported by concrete structures (bridges or culverts).

Figure 2. Path of HSR project in Egypt

One of the investigated elements is a pile cap located in the El Badrasheen Sector (HSR project). The rectangular pile cap of the bridge (9.6 × 13.2 × 3.0 m) is considered a mass concrete member as the depth of the pile cap (3.00 m) is the critical dimension. The second pile cap is located in October Sector (HSR project), with the same dimensions as the first pile cap, as shown in Figure 3. Consequently, their construction and early-age temperature profile were monitored and analyzed. The temperature development in a mass concrete structure is affected by many factors, such as the soil profile, environmental and boundary conditions, concrete mix design and proportions, and cooling method, as discussed previously. Therefore, the pile caps were studied before, during, and after the placement of concrete. Some of the significant information regarding these pile caps is presented and discussed in the next sections.

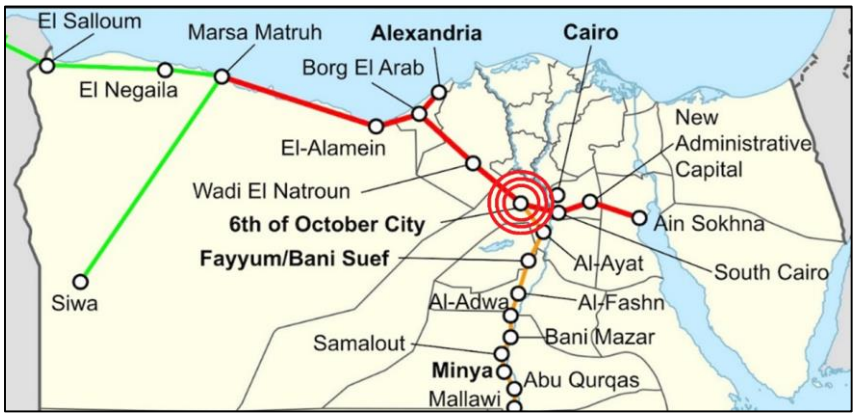

Figure 3. Location of the investigated pile cap in October Sector (HSR project)

4.2. Project Specifications

According to the project's specifications [40], a large pour is where the least dimension of the concrete element is greater than 1.35m. The contractor must take special measures with large pours to control temperature differences within the following limits:

- The temperature of the concrete at the time of placement must not exceed 22°C.
- The peak hydration temperature should not override 70°C. If the temperature overrides 70°C, the related part of the concrete must be demolished.
- The rise in temperature during hydration must not exceed 40°C.
- The difference in temperatures between any concrete face and the interior of the concrete at a distance of one

meter from that face should not exceed 15°C at any stage after the placement of concrete.

- The concrete temperature must be recorded at intervals not exceeding 6 hours for 7 days.

To insulate and protect the concrete surface, the formwork should be lined with insulating materials, and the surface of the concrete should be protected as soon as possible after the initial set has taken place. This should be accomplished by covering the concrete surface with 100 mm of sand kept continuously wet for 10 days.

4.3. Temperature Monitoring

Thermal sensors are usually used to monitor the temperature of the internal core and external surface of the concrete to make sure that the temperature differences are within the accepted limits. At least six temperature sensors are required for each mass concrete pour, with one sensor at the center of mass, as indicated by Bobko et al. [41]. For the investigated pile caps, 18 thermocouple probes (K type with a resolution of 0.1°C/1.0°C) were installed in concrete. This allowed for the monitoring of the temperatures generated by the exothermic reaction of the cement during casting and the maturity period of the concrete in the structure. Each pile cap was instrumented with a total of 9 thermocouples (K-type) at the top, middle, and bottom levels in the left, center, and right sections of the pile cap, as shown in Figure 4.

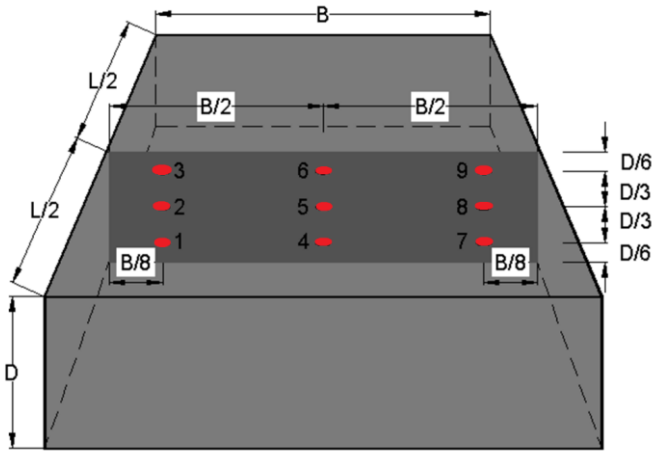

Figure 4. Thermocouple probes (K-type) locations in the pile caps

Continuous temperature monitoring was carried out every 3 or 6 hours for 7 days once the pouring of the concrete started (from 1:00 PM 8th of June 2022 to 10:00 AM 15th of June 2022). Figure 5 presents the used temperature measurement tools for concrete before pouring and after hardening.

(a) (b)

Figure 5. Measuring the temperature of concrete using the display unit

4.4. Materials and Mix Proportions

The concrete mix was designed to reach the required compressive strength of 450 kg/cm^2 after 28 days with a slump of 220 ± 20 mm. Ice was used to ensure that the temperature of the fresh concrete will not exceed the specified temperature of 22°C before pouring.

The used materials are natural siliceous sand (fine aggregates), two sizes of dolomite crushed stones (12.5 and 19mm) (coarse aggregates), potable water, low heat cement (CEM III - 42.5 N), and two types of super-plasticizers

Ha-Be-Fm240 (added to produce high-quality concrete), and NitCal50 (added to avoid corrosion). Table 1 summarizes the used proportions of the concrete mix.

Table 1. The used concrete mix proportions

Item	Weight (kg/m^3)
Cement (Type CEM III)	450
Crushed stone19.0 mm	490
Crushed stone12.5 mm	575
Sand	710
Total Aggregates	1775
Free Water	55
Ice	120
Total weight of Water	175
Ha-Be - Fm 240	7.5
Ha-Be - NitCal 50	8.0
Total plasticizers	15.5
Total weight	2415.5

The initial slump for this mix was 24 cm, and the initial setting time was 7 hours. The compressive strength of the standard 150 mm cube was measured at ages 3, 7, and 28 days, and the results were 36.5, 48.0, and 55.0 MPa, respectively.

4.5. Measurements

The temperature degrees at each sensor location, besides the air degrees, were recorded every three or six hours for seven days. The initial temperature degree of the fresh concrete was measured during casting, and it was 13.3 °C, as shown in Figure 5-a. The recorded measurements showed that the air temperatures ranged between 25 and 37 °C (the average temperature is 31±6 °C). The maximum and minimum values almost occurred at 4:00 PM and 4:00 AM, respectively. The maximum and minimum recorded degrees at the edge of the cap were (25 and 61 °C) for top-level, (26 and 66 °C) for mid-level, and (24 and 42 °C) for bottom-level. Similarly, the measured degrees at the center of the cap were (38 and 50 °C) for top-level, (27 and 68 °C) for mid-level, and (25 and 44 °C) for bottom-level. The maximum degree was recorded at 42 and 60 hours after casting for the edge and the center of the pile cap, respectively.

5. Analytical Methodology

The basic partial differential equation for heat transfer in three dimensions is very simple and could be defined as follows:

"For a finite volume element, the sum of the input heat rate in all directions subtract the sum of the output heat rate in all directions plus the generated heat rate within the element equals the storage heat rate in the element". Figure 6 shows the heat rate (Q') through a finite volume element, while Equation 1 presents the basic partial differential equation for heat transfer.

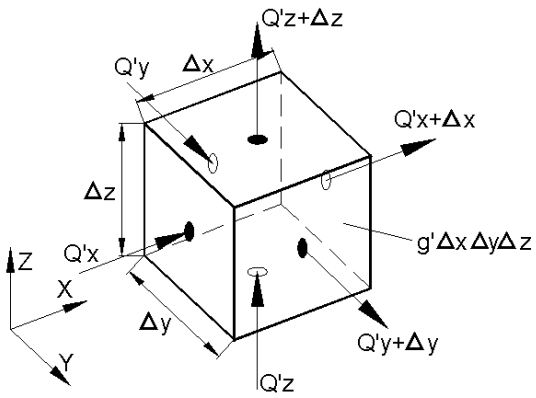

Figure 6. Heat rate (Q') through a finite volume element

$$\frac{\partial T}{\partial t} = \alpha\left(\frac{\partial^2 T}{\partial x^2} + \frac{\partial^2 T}{\partial y^2} + \frac{\partial^2 T}{\partial z^2} + \frac{\dot{q}}{k}\right) \quad (1)$$

where T is Temperature in (K), t is Time in (sec), x,y,z are Coordinates in (m), k is Thermal conductivity in W/(m.K), α is Thermal diffusivity (m^2/sec) = k/(ρ.c), ρ is Density in (kg/m^3), c is Specific heat J/(kg.K), and $\dot{q}$ is Volumetric rate of heat generation (W/m^3).

To solve this partial differential equation numerically, the 3D Finite Difference technique is used. The equivalent finite difference equation for heat transfer in three dimensions is illustrated in Figure 7 and presented in Equation 2.

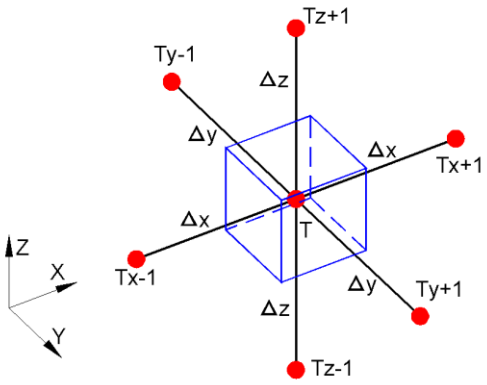

Figure 7. Typical 3D- finite difference node annotations

$$T_{n+1} = T_n + \frac{\Delta t.\alpha}{\Delta^2}\left(T_{n.X+1} + T_{n.X-1} + T_{n.y+1} + T_{n.y-1} + T_{n.z+1} + T_{n.z-1} - 6T_n + \frac{\dot{q}_n}{k}\right) \quad (2)$$

where Δ is Coordinate interval Δ = Δx = Δy =Δz, Δt is Time interval, n is Considered time step, T_n is Temperature degree at time step (n) at the considered node, T_{n+1} is Temperature degree at time step (n+1) at the considered node, $T_{n,x+}1$ is Temperature degree at time step (n) at the node next to the considered node in X-direction, similarly $T_{n,y+1}$ and $T_{n,z+1}$ in Y and Z directions, $T_{n,x-1}$ is Temperature degree at time step (n) at the node before the considered node in X-direction, similarly $T_{n,y-1}$ and $T_{n,z-1}$ in Y and Z directions, and $\dot{q}_n$ is Volumetric rate of heat generation at time step (n) at the considered node.

5.1. Concrete Properties

The most direct way to reduce the temperature rise in concrete is by reducing the cement content in the concrete mix design. Unfortunately, this is not applicable in most cases due to durability and strength restrictions. The thermal properties that are used to determine concrete temperature are density, thermal conductivity, specific heat, and convective heat transfer coefficients. These properties rely on the age of the concrete and temperature, w/c, cement type, aggregate type, and unit weight [42-44].

The considered concrete properties in this research were selected within the recommended ranges for structural concrete in the ACI-122R-02 "Guide to Thermal Properties of Concrete and Masonry Systems" [45], as listed in Table 2.

Table 2. The considered thermal properties of the used materials

Property	Symbol	Unit	Min.	Max.	Selected
Density	ρ	kg/m^3	2200	2400	2300
Thermal conductivity	k	W/(m.K)	1.2	3.2	2.6
Specific heat	c	J/(kg.K)	820	920	850
Thermal diffusivity	α	m^2/sec	$0.7x10^{-6}$	$1.45x10^{-6}$	$1.30x10^{-6}$

5.2. Heat of Hydration for Cement (q)

The heat of hydration value mainly depends on the chemical composition of cement [46]. For CEM I (OPC) at 20ºC, (q) varied between 300, 350 and 400 kJ/kg at 3, 7 and 28 days respectively. While the values are 230, 250, 270 kJ/kg for CEM III (Low heat) at 3, 7 and 28 days respectively. Equation 3 presents a hyperbolic model for the heat of hydration with time at 20ºC for CEM III.

$$\text{Heat of hydration (q)}\left(\frac{\text{J}}{\text{kg}}\right) = \frac{1000\,000\,\text{t}}{3.6\,\text{t}+205\,000} \quad (3)$$

where (t) in sec.

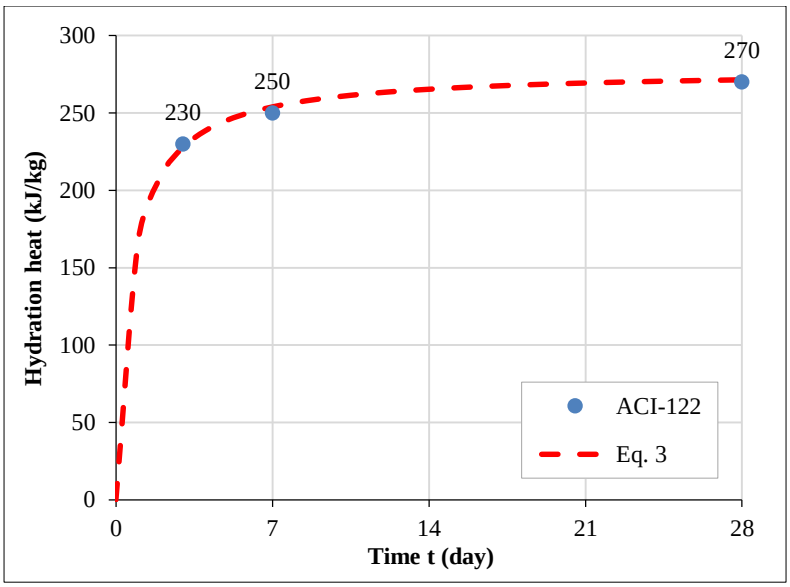

Figure 8. (Time-Hydration heat) relation for CEM III at 20 ºC and the proposed hyperbolic regression as per Equation 3

Hence, the volumetric rate of heat generation of concrete (q·) is the differentiation of Equation 3 multiplied by the cement content in the concrete mix as shown in Equation 4.

$$q\cdot\left(\frac{W}{m^3}\right)=\frac{205x10^9\ C}{(3.6\ t+205\ 000)^2} \quad (4)$$

where (t) in sec, (C) cement content kg/m^3.

5.3. Air Temperature (T air)

Apparent temperature of air varied between the maximum value at noon and the minimum value at midnight. Equation 5 presents the mathematical formula for air's temperature (T_{air}) along the day [47].

$$T_{air}=\left(\frac{T_{max}+T_{min}}{2}\right)-\left(\frac{T_{max}-T_{min}}{2}\right)sin\left(\frac{\pi\,(2t+t_{min})}{24}\right) \quad (5)$$

where T_{air} is Apparent temperature of air at certain clock time (t), where (0 < t < 24), T_{max} is Maximum apparent temperature along the day, T_{min} is Minimum apparent temperature along the day, and t_{min} is The clock time at minimum temperature (T_{min}).

5.4. Convective Heat Flux (q'c)

Convective heat flux is the transferred thermal energy from concrete surface to the surrounding air per unit (W/m^2). The amount of dissipated energy depends on the temperature difference between concrete surface and surrounding air, and also the wind speed [48]. Kuriakose et al. [47] presented Equation 6 to estimate the convective heat flux.

$$q'c\ \left(\frac{W}{m^2}\right)=hc\ \left(T_{surface}-T_{air}\right) \quad (6)$$

where $hc=\begin{matrix}5.6+3.95\ v & for\ v\le 5.0\ m/s^2\\ 7.6\ v^{0.78} & for\ v>5.0\ m/s^2\end{matrix}$

5.5. The Developed 3D-Finite Difference Model

The developed model is carried out using MS-Excel software. It consists of a homogenous concrete block 10.0x13.0x3.0m rested on the soil and exposed to air temperature but not exposed to direct sunlight (no heat radiation or irradiation). The selected concrete properties in Table 2 were considered for all elements. The selected mesh size was 1.0m in all directions, which means four layers of nodes; each layer contains (11x14 nodes), which is a total of 616 nodes. A 10800-second (three-hour) time step was selected to satisfy the iteration stability as per Equation7.

$$\Delta t\ \le\frac{\Delta^2}{8\ \alpha}=\frac{1.0}{10.8\times10^{-6}}=92600sec \quad (7)$$

The rate of hydration heat generated for each element was calculated using Equation 4 where the cement content (C) equals 450 kg/m^3. The surface and corner nodes simulate half and quarter elements, and hence they generate half and quarter hydration heat rates, respectively.

5.6. Initial and Boundary Conditions

As recorded, the initial temperature of the casted concrete was 13°C and the recording started at 1:00 PM. The temperatures of all exposed surfaces were equal to the air temperature and followed Equation 5 considering T_{min} and T_{max} equal to 25 and 37°C respectively, and the time at the minimum temperature (t_{min}) was 4:00 AM. Besides, all exposed surfaces were subjected to a wind speed of 10 m/s as measured by an anemometer, accordingly, the convective heat flux (q'c) on these surfaces was 45 W/m^2 as per Equation 6. Finally, the temperature of the bottom surface (which is in contact with soil) was kept constant and equal to 31°C (as the average temperature of air).

6. Results and Discussion

For the pile cap in El Badrasheen Sector, 56-time steps were calculated as per Equation 2, which is equivalent to 168 hours or 7 days after casting. The peak temperature at the center of the block (65°C) occurred at time step 20 (60 hours after casting) at 1:00 AM, where the air temperature was 26°C and the surface temperature was 32°C. Figure 9 presents the temperature contours for the top, middle, and bottom surfaces of the block at time steps 20 and 54, where the outer frame is the air temperature.

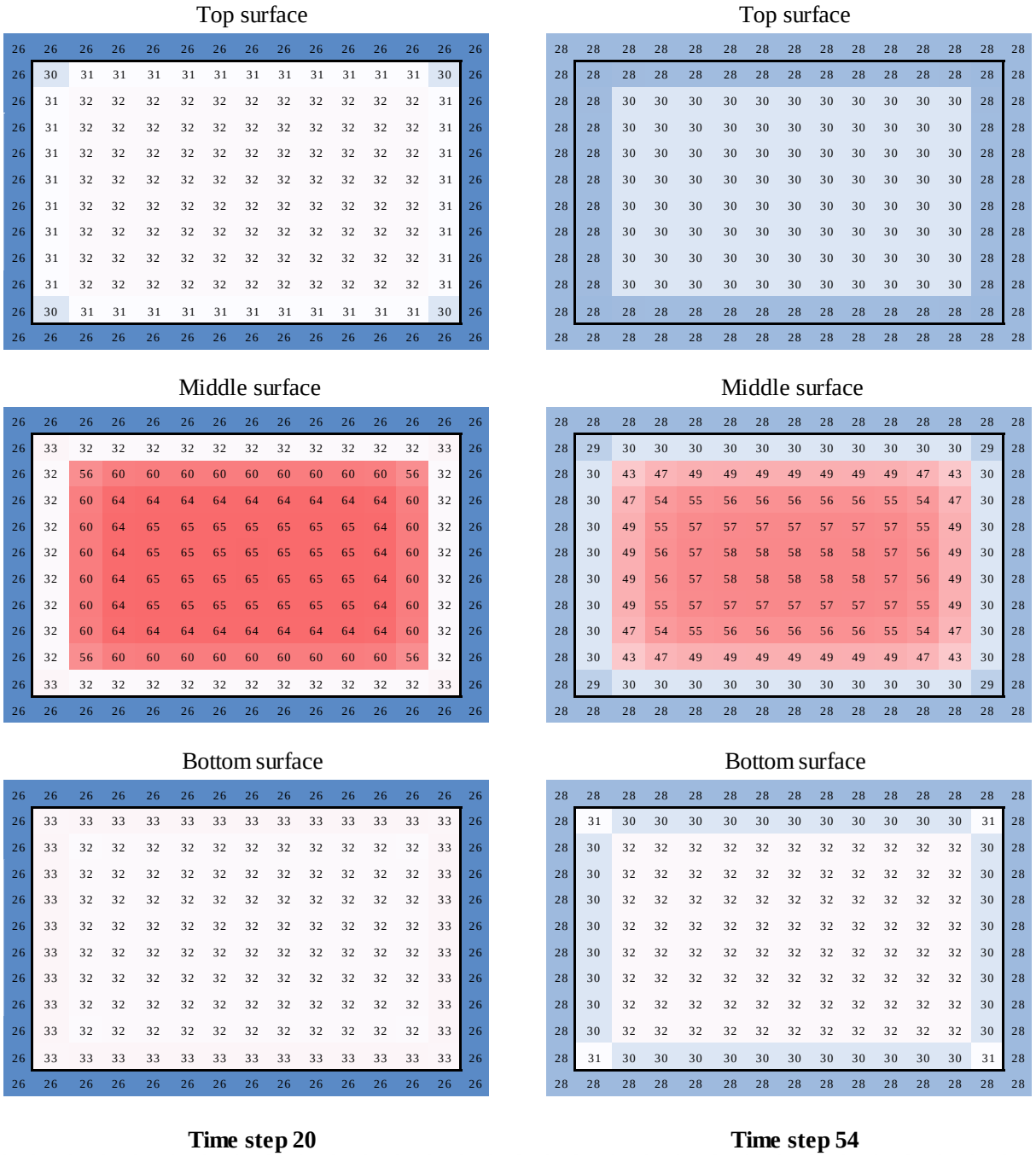

Figure 9. Temperature contours for the top, middle, and bottom surfaces of the block at time steps 20 and 54, where the outer frame is the air temperature at El Badrasheen Sector

For the pile cap in October Sector, 28 time steps were calculated as per Equation 2, which is equivalent to 168 hours or 7 days after casting. The peak temperature at the center of the block (63 ^{o}C) occurred at time step 10 (60 hours after casting) at 2:30 PM, where the air temperature was 28 ^{o}C and the surface temperature was 31^{o}C. Figure 10 presents the temperature contours for the top, middle, and bottom surfaces of the block at time steps 10 and 28, where the outer frame is the air temperature.

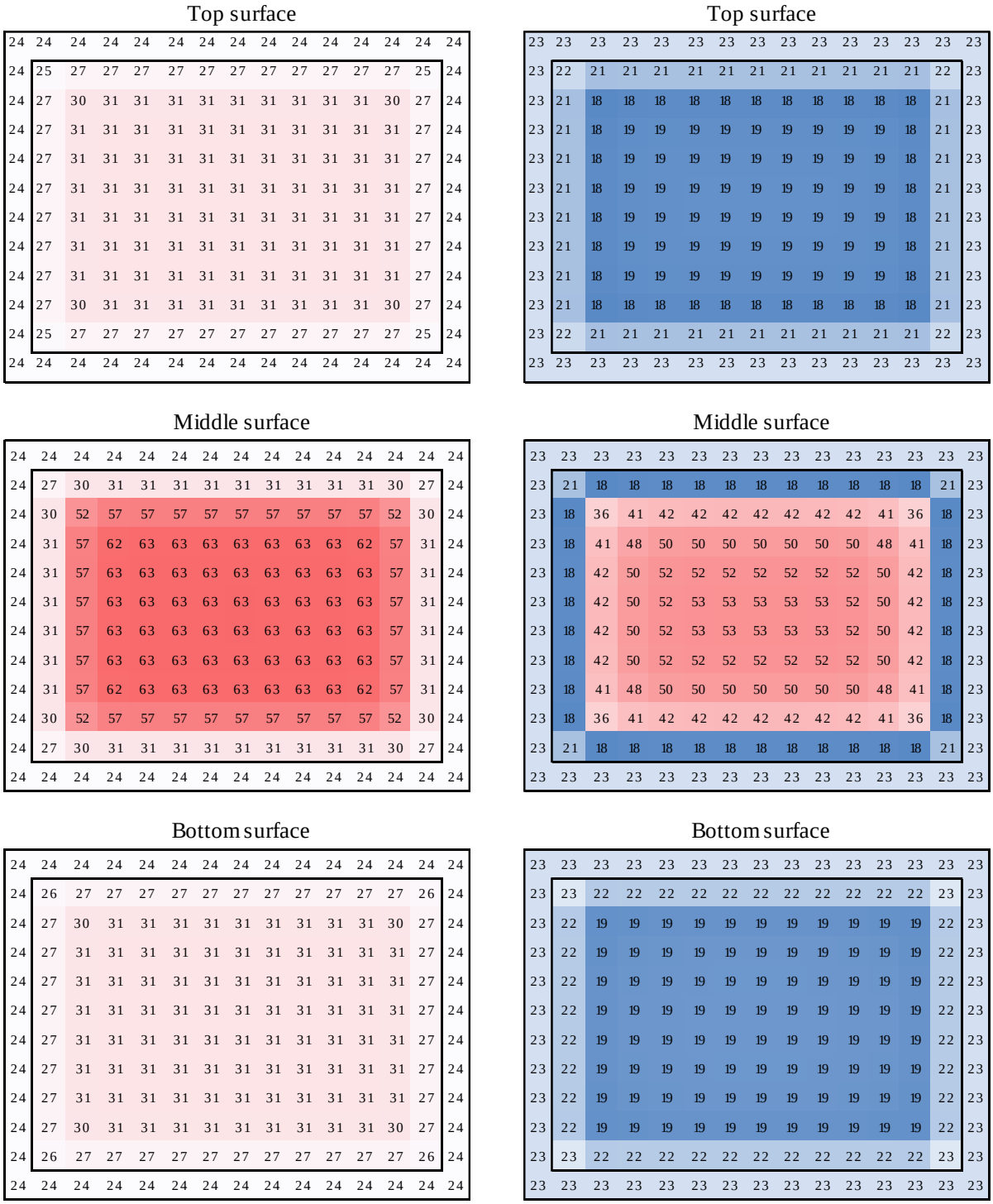

Figure 10. Temperature contours for the top, middle, and bottom surfaces of the block at time steps 10 and 28, where the outer frame is the air temperature at October Sector

To compare the calculated temperatures with the measured ones (at a depth of 0.5m below the concrete surface), the average temperature of a surface node and an adjacent one is considered. Figures 11 and 12 present a comparison between calculated and measured temperatures at different points besides the considered and actual air temperatures.

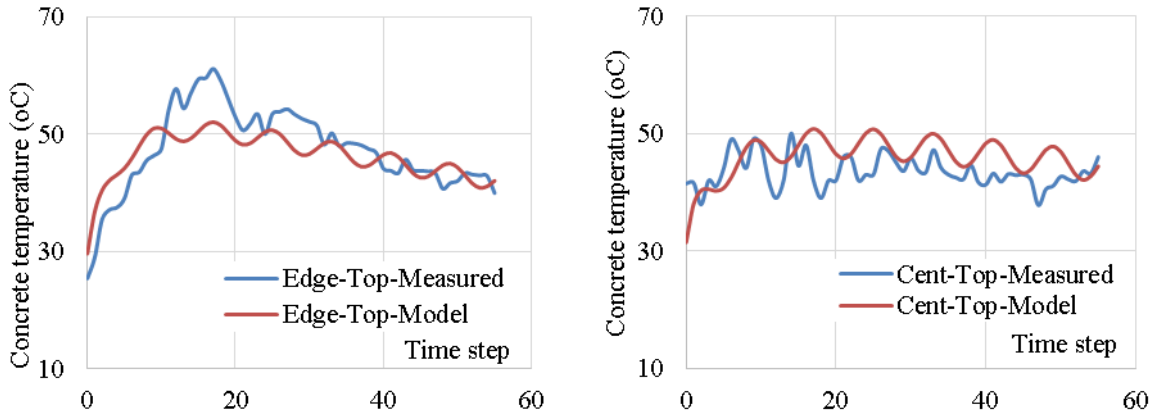

(a). Edge of top level

(b). Center of top level

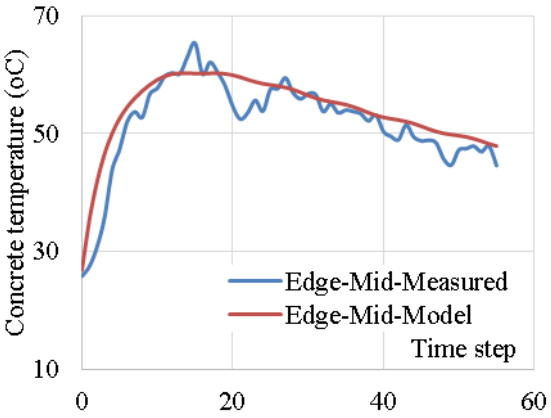

(c). Edge of middle level

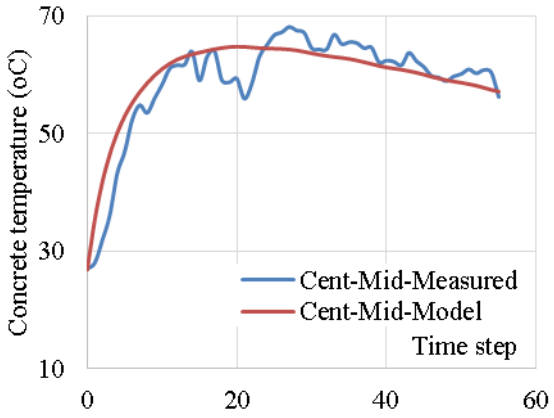

(d). Center of middle level

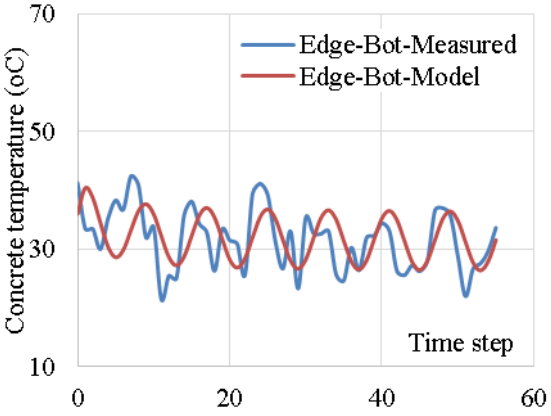

(e). Edge of bottom level

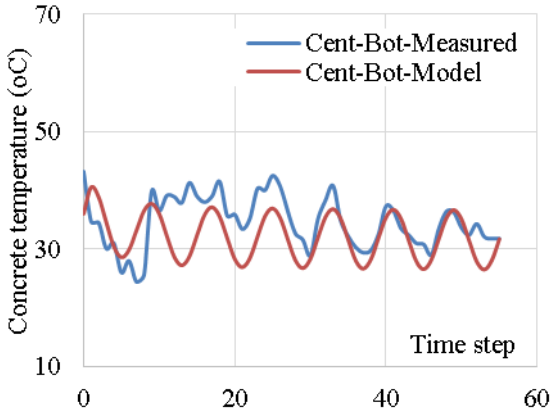

(f). Center of bottom level

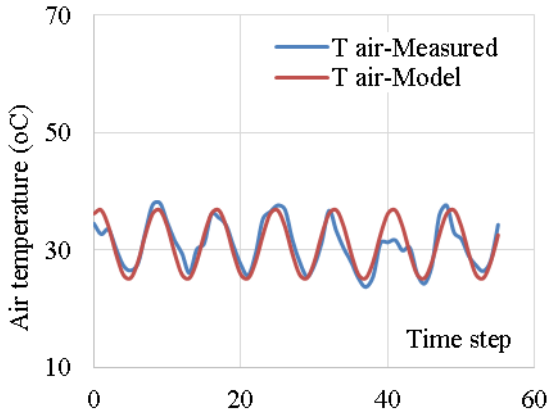

(g). Air temperature

Figure 11. Comparison between calculated and measured temperatures at different locations at El Badrasheen Sector

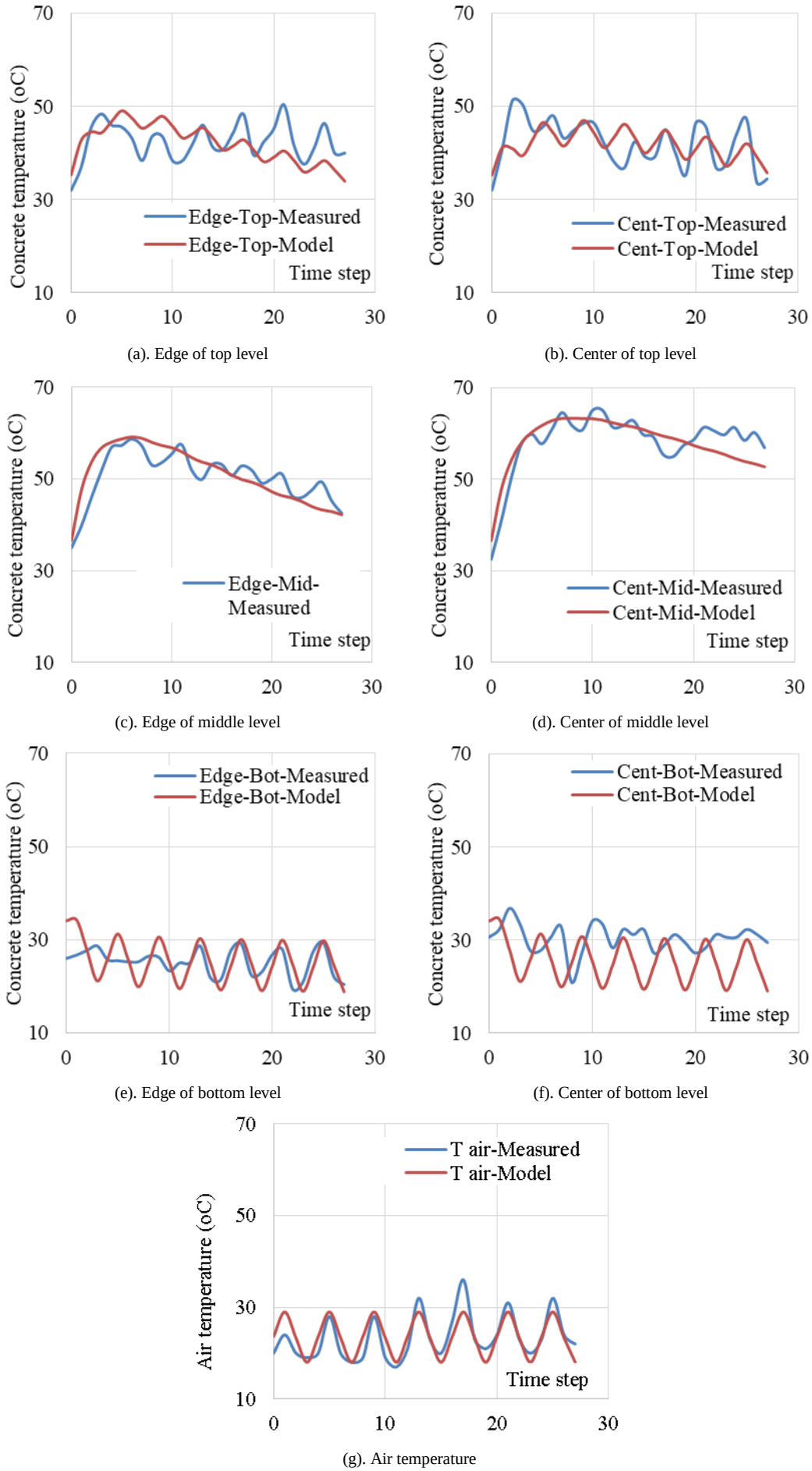

(a). Edge of top level

(b). Center of top level

(c). Edge of middle level

(d). Center of middle level

(e). Edge of bottom level

(f). Center of bottom level

(g). Air temperature

Figure 12. Comparison between calculated and measured temperatures at different locations at October Sector

The comparison charts shown in Figures 11 and 12 illustrate that the temperature prediction accuracies are about ±5%, ±8%, ±6%, and ±12% for the air, top, middle, and lower surfaces of the pile caps, respectively, and the maximum difference between the calculated and measured temperature degrees is about 5 °C and 10 °C for the air and concrete, respectively. Most of these extreme differences occurred due to a slight shifting (or delay) in the temperature cycle, as in Figures 11-a and 11-e, or due to random or local variation, as in Figures 11-c, 11-d, and 11-f. However, it could be generally noted that the calculated temperature is slightly higher than the measured temperature at the top surface (Figures 11-a and 11-b) and slightly lower at the bottom surface (Figures 11-e and 11-f), especially at the center of the pile cap. Figures 11 and 12 display the variation of concrete temperature degrees on the top and bottom surfaces of the pile caps due to their direct contact with fluctuating temperature surfaces (air or soil). On the other hand, these figures present the average temperature inside the pile caps, where the generated heat is trapped. The temperature prediction accuracies are about ±10% (±3.5°C) for air and exposed concrete surfaces due to temperature variation, while they are about ±5% (±3.5°C) for inside concrete, where the variation decreases.

7. Conclusion

The results of this research prove that the proposed 3D-Finite Difference Model can be used to solve the partial differential equation that governs heat transfer and determine the temperature distribution within massive concrete pile caps. The comparison charts between the developed model values and the site measurements confirmed that the FDM captured the fluctuation of concrete temperature degrees on the top and bottom surfaces of the pile caps due to their contact with fluctuating temperature surfaces, while the model captured only the average temperature inside the pile caps, where the generated heat is trapped. The temperature prediction accuracies are about ±10% for air and exposed concrete surfaces due to temperature fluctuation, while they are about ±5% for inside concrete, where the fluctuation decreases.

The proposed model provides useful information to make critical construction decisions, such as insulation practices, formwork removal time, precooling and post cooling techniques, and minimizing the risk of early-age thermal cracking in mass concrete structures. In order to prevent thermal cracking, concrete element temperature histories should be predicted during the design and construction phases. Using the concrete mixture data and cement properties, this research shows that the temperature predictions can be reasonably well correlated with the site data.

8. Declarations

8.1. Author Contributions

Conceptualization, D.M. and A.E.; methodology, A.E.; software, A.E.; validation, D.M. and A.E.; formal analysis, A.E.; investigation, D.M.; resources, D.M.; data curation, D.M.; writing—original draft preparation, D.M. and A.E.; writing—review and editing, D.M. and A.E.; visualization, A.E.; supervision, A.E.; project administration, D.M.; funding acquisition, D.M. All authors have read and agreed to the published version of the manuscript.

8.2. Data Availability Statement

The data presented in this study are available on request from the corresponding author.

8.3. Funding

The authors received no financial support for the research, authorship, and/or publication of this article.

8.4. Acknowledgements

The authors would deeply like to acknowledge the assistance presented by SAMCO and Hassan Allam Company. Special thanks are extended as well to the General Authority for Roads, Bridges, and Land Transportation (GARBLT) and the National Authority for Tunnels (NAT) of Egypt. The assistance received from the project manager, Ahmed Mousad, from the High-Speed Railway (HSR) project (El Badrasheen Sector) is especially acknowledged.

8.5. Conflicts of Interest

The authors declare no conflict of interest.

9. References

[1] Guo, C., & Lu, Z. (2020). Effect of temperature on CFST arch bridge ribs in harsh weather environments. Mechanics of Advanced Materials and Structures, 29, 1–16. doi:10.1080/15376494.2020.1790701.

[2] Fan, J. S., Li, B. L., Liu, C., & Liu, Y. F. (2022). An efficient model for simulation of temperature field of steel-concrete composite beam bridges. Structures, 43, 1868–1880. doi:10.1016/j.istruc.2022.05.079.

[3] ACI 116R-00. (2005). Cement and Concrete Terminology. American Concrete Institute (ACI), Michigan, United States.

[4] da Amorim Coelho, N., Pedroso, L. J., da Silva Rêgo, J. H., & Nepomuceno, A. A. (2014). Use of ANSYS for Thermal Analysis in Mass Concrete. Journal of Civil Engineering and Architecture, 8(7), 860–868. doi:10.17265/1934-7359/2014.07.007.

[5] Shawkey, M. A., Hassan, A. M., & Rashad, M. M. (2022). Numerical Analysis of Thermal Cracking Estimation of Mass Concrete With GGBS at an Early Age. Egyptian Journal of Chemistry, 65(5), 193–205. doi:10.21608/ejchem.2021.97424.4554.

[6] Mansour, D. M., & Ebid, A. M. (2023). Predicting thermal behavior of mass concrete elements using 3D finite difference model. Asian Journal of Civil Engineering. doi:10.1007/s42107-023-00864-2.

[7] Yikici, T. A., Sezer, H., & Chen, H. L. (2022). Modeling Thermal Behavior of Mass Concrete Structures at Early Age. Transportation Research Record, 2676(6), 536–548. doi:10.1177/03611981221075626.

[8] Bartojay, K. (2012). Thermal properties of reinforced structural mass concrete. Dam Safety Technology Development Program, Bureau of Reclamation, Denver, United States.

[9] Klemczak, B., & Żmij, A. (2021). Insight into thermal stress distribution and required reinforcement reducing early-age cracking in mass foundation slabs. Materials, 14(3), 1–19. doi:10.3390/ma14030477.

[10] Xu, Z. H., Sun, D. W., & Xiao, H. (2012). Finite Element Analysis of Mass Concrete Temperature Crack Mechanism. Advanced Materials Research, 594–597, 713–716. doi:10.4028/www.scientific.net/amr.594-597.713.

[11] Zhang, T., Wang, H., Luo, Y., Yuan, Y., & Wang, W. (2023). Hydration Heat Control of Mass Concrete by Pipe Cooling Method and On-Site Monitoring-Based Influence Analysis of Temperature for a Steel Box Arch Bridge Construction. Materials, 16(7), 2925. doi:10.3390/ma16072925.

[12] Portland Cement Association. (1997). Portland cement, concrete, and heat of hydration. Concrete Technology Today, 18(2), 1-4.

[13] Kumar, K. A., Rajasekhar, K., & Sashidhar, C. (2022). Experimental Research on the Effects of Waste Foundry Sand on the Strength and Micro-Structural Properties of Concrete. Civil Engineering Journal, 8(10), 2172-2189. doi:10.28991/CEJ-2022-08-10-010.

[14] Onyelowe, K. C., Ebid, A. M., Ramani Sujatha, E., Fazel-Mojtahedi, F., Golaghaei-Darzi, A., Kontoni, D.-P. N., & Nooralddin-Othman, N. (2023). Extensive overview of soil constitutive relations and applications for geotechnical engineering problems. Heliyon, 9(3), e14465. doi:10.1016/j.heliyon.2023.e14465.

[15] ACI 207.R-05. (1997). Guide to Mass Concrete. American Concrete Institute (ACI), Michigan, United States.

[16] Rita, M., Fairbairn, E., Ribeiro, F., Andrade, H., & Barbosa, H. (2018). Optimization of Mass Concrete Construction Using a Twofold Parallel Genetic Algorithm. Applied Sciences, 8(3), 399. doi:10.3390/app8030399.

[17] Gajda, J. (2007). Mass concrete for buildings and bridges. Portland Cement Association, Washington, United States.

[18] Leon, G., & Chen, H. L. (2021). Thermal Analysis of Mass Concrete Containing Ground Granulated Blast Furnace Slag. CivilEng, 2(1), 254–270. doi:10.3390/civileng2010014.

[19] Marshall, A. L. (1972). The thermal properties of concrete. Building Science, 7(3), 167–174. doi:10.1016/0007-3628(72)90022-9.

[20] Aït Alaïwa, A., Thiebaut, Y., Linger, L., & Boutillon, L. (2022). Operational implementation of concrete thermal modeling for construction projects. Structural Concrete, 23(6), 3754–3771. Portico. doi:10.1002/suco.202100725.

[21] Han, S. (2020). Assessment of curing schemes for effectively controlling thermal behavior of mass concrete foundation at early ages. Construction and Building Materials, 230, 117004. doi:10.1016/j.conbuildmat.2019.117004.

[22] Liu, X., Zhang, C., Chang, X., Zhou, W., Cheng, Y., & Duan, Y. (2015). Precise simulation analysis of the thermal field in mass concrete with a pipe water cooling system. Applied Thermal Engineering, 78, 449–459. doi:10.1016/j.applthermaleng.2014.12.050.

[23] Yang, J., Hu, Y., Zuo, Z., Jin, F., & Li, Q. (2012). Thermal analysis of mass concrete embedded with double-layer staggered heterogeneous cooling water pipes. Applied Thermal Engineering, 35(1), 145–156. doi:10.1016/j.applthermaleng.2011.10.016.

[24] Maruyama, I., & Lura, P. (2019). Properties of early-age concrete relevant to cracking in massive concrete. Cement and Concrete Research, 123, 105770. doi:10.1016/j.cemconres.2019.05.015.

[25] Chu, I., Lee, Y., Amin, M. N., Jang, B. S., & Kim, J. K. (2013). Application of a thermal stress device for the prediction of stresses due to hydration heat in mass concrete structure. Construction and Building Materials, 45, 192–198. doi:10.1016/j.conbuildmat.2013.03.056.

[26] Chen, H. L. (Roger), Mardmomen, S., & Leon, G. (2021). On-site measurement of heat of hydration of delivered mass concrete. Construction and Building Materials, 269. doi:10.1016/j.conbuildmat.2020.121246.

[27] Dam Safety Program Technology Development. (2017). Comparison of Thermal Property Models for Concrete, Geotechnical, and Structural Laboratory. U.S. Department of the Interior Bureau of Reclamation, Washington, United States.

[28] ACI 207. 2R-07. (2007). Report on Thermal and Volume Change Effects on Cracking of Mass Concrete. American Concrete Institute (ACI), Michigan, United States.

[29] Bobko, C. P., Zadeh, V. Z., & Seracino, R. (2015). Improved Schmidt Method for Predicting Temperature Development in Mass Concrete. ACI Materials Journal, 112(4), 579–586. doi:10.14359/51687454.

[30] Abeka, H., Adom-Asamoah, M., Osei Banahene, J., & Adinkrah-Appiah, K. (2018). Temperature prediction models in mass concrete state of the art literature review. 1st International Conference on Engineering, Science, Technology and Entrepreneurship (ESTE), 6-7 August, 2015, Kumasi, Ghana.

[31] Zhu, F., Chen, G., Zhang, F., & Li, Q. (2021). Numerical Simulation of Thermal Field in Mass Concrete with Pipe Water Cooling. Frontiers in Physics, 9. doi:10.3389/fphy.2021.716859.

[32] Huang, Y., Liu, G., Huang, S., Rao, R., & Hu, C. (2018). Experimental and finite element investigations on the temperature field of a massive bridge pier caused by the hydration heat of concrete. Construction and Building Materials, 192, 240–252. doi:10.1016/j.conbuildmat.2018.10.128.

[33] Do, T., Lawrence, A., Tia, M., & Bergin, M. (2013). Importance of insulation at the bottom of mass concrete placed on soil with high groundwater. Transportation Research Record, 2342(2342), 113–120. doi:10.3141/2342-14.

[34] Sargam, Y., Faytarouni, M., Riding, K., Wang, K., Jahren, C., & Shen, J. (2019). Predicting thermal performance of a mass concrete foundation – A field monitoring case study. Case Studies in Construction Materials, 11, 289–305. doi:10.1016/j.cscm.2019.e00289.

[35] Lin, Y., & Chen, H. L. (2015). Thermal analysis and adiabatic calorimetry for early-age concrete members. Journal of Thermal Analysis and Calorimetry, 122(2), 937–945. doi:10.1007/s10973-015-4843-2.

[36] Lawrence, A. M., Tia, M., Ferraro, C. C., & Bergin, M. (2012). Effect of Early Age Strength on Cracking in Mass Concrete Containing Different Supplementary Cementitious Materials: Experimental and Finite-Element Investigation. Journal of Materials in Civil Engineering, 24(4), 362–372. doi:10.1061/(asce)mt.1943-5533.0000389.

[37] Yikici, T. A., & Chen, H.-L. (Roger). (2015). Numerical Prediction Model for Temperature Development in Mass Concrete Structures. Transportation Research Record: Journal of the Transportation Research Board, 2508(1), 102–110. doi:10.3141/2508-13.

[38] Mahdi, I. M., Khalil, A. H., Mahdi, H. A., & Mansour, D. M. M. (2022). Decision support system for optimal bridge' maintenance. International Journal of Construction Management, 22(3), 342–356. doi:10.1080/15623599.2019.1623991.

[39] Mohamed Mansour, D. M., Moustafa, I. M., Khalil, A. H., & Mahdi, H. A. (2019). An assessment model for identifying maintenance priorities strategy for bridges. Ain Shams Engineering Journal, 10(4), 695–704. doi:10.1016/j.asej.2019.06.003.

[40] The National Research Centre for Housing and Building. (2018). The Egyptian Code for Design and Construction of Reinforced Concrete Structures 203-2018. The National Research Centre for Housing and Building, Cairo, Egypt.

[41] Bobko, C. P., Seracino, R., Zia, P., Edwards, A., & Hall, M. (2014). Crack Free Mass Concrete Footings on Bridges in Coastal Environments. North Carolina State University, Raleigh, United States.

[42] Yeon, J. H., Choi, S., & Won, M. C. (2013). In situ measurement of coefficient of thermal expansion in hardening concrete and its effect on thermal stress development. Construction and Building Materials, 38, 306–315. doi:10.1016/j.conbuildmat.2012.07.111.

[43] Lee, M. H., Chae, Y. S., Khil, B. S., & Yun, H. D. (2014). Influence of Casting Temperature on the Heat of Hydration in Mass Concrete Foundation with Ternary Cements. Applied Mechanics and Materials, 525, 478–481. doi:10.4028/www.scientific.net/amm.525.478.

[44] Asadi, I., Shafigh, P., Abu Hassan, Z. F. Bin, & Mahyuddin, N. B. (2018). Thermal conductivity of concrete – A review. Journal of Building Engineering, 20, 81–93. doi:10.1016/j.jobe.2018.07.002.

[45] ACI 122R-02. (2002). Guide to Thermal Prosperities of Concrete and Masonry Systems. American Concrete Institute (ACI), Michigan, United States.

[46] Livesey, P., Donnelly, A., & Tomlinson, C. (1991). Measurement of the heat of hydration of cement. Cement and Concrete Composites, 13(3), 177–185. doi:10.1016/0958-9465(91)90018-D.

[47] Kuriakose, B., Rao, B. N., Dodagoudar, G. R., & Venkatachalapathy, V. (2015). Modelling of heat of hydration for thick concrete constructions - A note. Journal of Structural Engineering (India), 42(4), 348–357.

[48] Ebid, A. M., Onyelowe, K. C., Kontoni, D.-P. N., Gallardo, A. Q., & Hanandeh, S. (2023). Heat and mass transfer in different concrete structures: a study of self-compacting concrete and geopolymer concrete. International Journal of Low-Carbon Technologies, 18, 404–411. doi:10.1093/ijlct/ctad022.